

From Perception to Symbolic Task Planning: Vision-Language Guided Human-Robot Collaborative Structured Assembly

Yanyi Chen, Min Deng*

Abstract—Human-robot collaboration (HRC) in structured assembly requires reliable state estimation and adaptive task planning under noisy perception and human interventions. To address these challenges, we introduce a design-grounded human-aware planning framework for human-robot collaborative structured assembly. The framework comprises two coupled modules. **Module I**, Perception-to-Symbolic State (PSS), employs vision-language models (VLMs) based agents to align RGB-D observations with design specifications and domain knowledge, synthesizing verifiable symbolic assembly states. It outputs validated installed and uninstalled component sets for online state tracking. **Module II**, Human-Aware Planning and Replanning (HPR), performs task-level multi-robot assignment and updates the plan only when the observed state deviates from the expected execution outcome. It applies a minimal-change replanning rule to selectively revise task assignments and preserve plan stability even under human interventions. We validate the framework on a 27-component timber-frame assembly. The PSS module achieves 97% state synthesis accuracy, and the HPR module maintains feasible task progression across diverse HRC scenarios. Results indicate that integrating VLM-based perception with knowledge-driven planning improves robustness of state estimation and task planning under dynamic conditions.

Index Terms—human-robot collaboration, vision-language models, structural frame assembly, multi-robot task allocation, symbolic planning

I. INTRODUCTION

STRUCTURED assembly, such as the construction of timber-frame building components, presents a significant challenge for robotic automation [1]. While robots excel at repetitive tasks in controlled environments, their deployment in the real world remains challenging due to dynamic site conditions, execution failures, and unscripted human interventions [2]. Unlike fully scripted industrial tasks, structured assembly tasks are characterized by evolving partial structures, strong precedence constraints, and incomplete observability during execution [3]. Components are installed incrementally, and the physical configuration of the structure changes continuously as assembly progresses. Moreover, humans work alongside robots and may perform unrecorded actions, such as temporarily fixing or installing components, further increasing uncertainty in the system state [4].

The first challenge concerns robust state estimation, which requires inferring the assembly state from real-world observations. In structured assembly, the state does not refer to

precise geometric poses, but to a component-level understanding of which parts have been installed, which remain uninstalled, and how the current configuration relates to the design specification. However, visual observations are often noisy and incomplete due to occlusions by workers, temporary fixtures, partial views of large structures, and sensing artifacts, making it difficult to reliably infer discrete assembly states from raw perception [5], [6]. The second challenge concerns adaptive task planning under structured assembly constraints. Based on the current symbolic state, the system must dynamically generate and revise actions for a heterogeneous human-robot team while preserving the structural validity of the assembly. In structured assembly, task admissibility and ordering are governed by domain-specific construction rules, such as support dependencies and precedence relations defined in the design specification [4], [7]. Human interventions can violate these assumptions by completing components out of order, removing supporting elements, or modifying the set of admissible components, thereby invalidating previously feasible plans. Naïve replanning strategies that regenerate plans from scratch ignore these structural dependencies and may unnecessarily reassign unaffected tasks, disrupt ongoing collaboration, and reduce plan stability in human-robot teams. These challenges lead to the following research questions:

- **RQ1:** How can a robotic system reconcile ambiguous and partially visual observations with a predefined design specification to produce a verifiable, component-level symbolic assembly state that is consistent with structural and construction constraints?
- **RQ2:** How can a task-level planning framework update and preserve coordinated human-robot assembly actions under unscripted human interventions, while respecting design-defined structural dependencies and minimizing unnecessary disruption to unaffected tasks?

To address these questions, we propose a closed-loop planning framework that combines design-grounded symbolic state synthesis with human-aware task planning. Human awareness in this paper is defined at the task and symbolic state level, where human actions are treated as exogenous events that modify the assembly state and trigger selective replanning. The framework maintains consistency between perceptual observations, design specifications, and planning decisions under perceptual uncertainty and unscripted human interventions.

The main contributions of this work are summarized as follows:

*Corresponding author

Yanyi Chen and Min Deng are with the Department of Civil, Environmental, and Construction Engineering, Texas Tech University, Lubbock, TX 79409, USA (e-mail: yanychen@ttu.edu, mindeng@ttu.edu)

- 1) We present a closed-loop, design-grounded planning framework that formalizes the interaction between symbolic state synthesis and human-aware task planning for robust human-robot collaborative assembly.
- 2) We propose a design-grounded symbolic state synthesis method that converts static design artifacts (e.g., DXF) into structured symbolic representations. By aligning vision-language model (VLM) inference with explicit engineering constraints, the method enables automated component-level state reasoning without manual semantic labeling.
- 3) We introduce a knowledge-driven human-aware task planning approach that determines valid next assembly actions and selectively updates task assignments in response to unscripted human interventions, without requiring full replanning.
- 4) We validate the proposed framework through a 27-component timber-frame wall assembly case study, demonstrating high symbolic state accuracy and reliable task progression under dynamic human-robot collaboration (HRC) scenarios.

The remainder of this paper is organized as follows. Section II reviews related work on knowledge-based assembly, foundation models in robotics, and human-robot collaborative planning. Section III presents the developed methodology, followed by the case study and experimental results in Section IV. Section V discusses implications and limitations, and Section VI concludes the paper.

II. RELATED WORK

A. Assembly Planning from Design Specifications

Assembly planning from design specifications extracts task representations from predefined models and knowledge structures, such as CAD files, graphical instructions, ontologies, and behavioral taxonomies. CAD-based approaches derive task representations from geometric and relational information in three-dimensional models, for example, by extracting part dependencies through liaison graph construction [8]. While they provide precise geometric information, they require complete CAD models and cannot handle assemblies documented only through visual instructions or manuals.

To overcome the reliance on complete CAD models, Wang et al. [9] propose extracting assembly task sequence graphs directly from graphical instruction manuals, enabling task reasoning when explicit design models are unavailable. Building on this direction, Lv et al. [10] extend manual-based parsing to multimodal scene graph representations that explicitly encode spatial relations among agents, objects, and assembly components.

Beyond visual parsing, explicit knowledge representations have been used to formalize assembly semantics and support symbolic planning. Zhao et al. [11] model products, processes, and resources using an intermediate engineering ontology that is translated into Planning Domain Definition Language (PDDL) for multi-agent task scheduling. In contrast, Angleraud et al. [12] adopt ontology-grounded Hierarchical Task

Networks (HTN) to generate collaborative assembly plans under predefined operators and constraints.

At a higher level, taxonomy and knowledge-based abstractions have been proposed to structure human-robot assembly skills. Lee et al. [13] introduce the human-robot shared assembly taxonomy framework. It decomposes tasks into primitive tasks and atomic actions to facilitate knowledge transfer between humans and robots. Conti et al. [14] incorporate commonsense knowledge to optimize task allocation based on safety and ergonomic constraints. To support skill generalization, Sun et al. [15] propose the multi-layer multi-level knowledge representation, structured across task, area, object, action, and agent layers. They utilize a knowledge-enhanced task-to-action model to reason about manipulation sequences and transfer skills between similar assembly objects. In parallel, learning-based approaches reduce manual modeling effort by extracting task representations from demonstrations, such as converting instructional videos into executable robot programs [16].

Despite differences in representation formalism, these methods share a common assumption that task representations derived from design artifacts align with physical assembly states. When physical configurations deviate from specifications, these frameworks cannot resolve the mismatch, often requiring manual intervention or replanning from scratch.

B. Foundation Models in Assembly

Foundation models have been introduced into robotic assembly to improve flexibility in task planning, typically by augmenting specific stages of the planning pipeline rather than replacing the full planning process.

Several studies employ Large Language Models (LLMs) for high-level task structure generation. For example, Bashir et al. [17] use LLMs to map visual observations to symbolic task states and predict subsequent assembly steps, while Macaluso et al. [18] leverage CAD-derived metadata to guide LLM-based generation of robot control programs. Ao et al. [19] further structure task execution by using behavior trees as an explicit control representation.

Other studies ground symbolic reasoning in physical environments to better handle real-world complexity. Specifically, Rana et al. [20] combine LLM-based semantic reasoning with hierarchical 3D scene graphs, enabling task planning that explicitly accounts for spatial structure. Similarly, You et al. [21] focus on assembly scenarios and infer task sequences under explicit spatial and resource constraints using symbolic planning. Forlini et al. [22] integrate multimodal perception to identify component states and update task plans when human interventions modify the workspace.

Beyond task generation, recent work addresses adaptation during execution to handle uncertainty. Kang et al. [23], for instance, extend HTN planning by translating natural language instructions into executable procedures, enabling contingency handling at the task level. Moreover, Hao et al. [24] propose the Learn-Gen-Plan framework, which leverages learned motion primitives and perception feedback to support long-horizon task adaptation. In construction contexts, Deng et

al. [25] integrate LLMs with Digital Twins to translate unstructured narrative site updates into constraint changes for multi-robot task allocation (MRTA).

In general, foundation models improve task adaptability in assembly planning. However, most existing methods assume that the perceived state used for planning is sufficiently accurate, without explicitly verifying consistency between perception outputs and the physical assembly state. Under incomplete or occluded observations, this assumption can lead to undetected mismatches between inferred task progress and actual execution, with limited mechanisms for correction.

C. Human-Robot Collaborative Planning

Research in human-robot collaborative planning spans a progression from behavioral modeling to real-time adaptation. Early work has focused on modeling human behavior to enable robots to anticipate and complement human interventions. Representative approaches include user-aware hierarchical task planning to monitor human progress and select robot actions without explicit communication [26], [27]. To manage the unpredictable nature of human behavior, Cramer et al. [28] applied Partially Observable Markov Decision Processes to estimate assembly intentions from state graphs. Similarly, Nemlekar et al. [29] used transfer learning to adjust robot assistance based on individual human habits observed in earlier tasks. While these methods enable intention inference and responsive robot behavior, they primarily focus on behavioral prediction and do not explicitly address task distribution among multiple agents.

Other studies focus on task allocation between humans and robots to balance efficiency with physical and geometric constraints. Examples include task allocation methods that consider part stability and geometric complexity [30], PDDL-based assignment considering reachability and safety [31], and discrete-event coordination using event-driven timing models [32]. Although these approaches improve coordination, task assignments are typically computed based on an initial workspace configuration and provide limited mechanisms for revision when the assembly state changes during execution.

To improve robustness during execution, several frameworks introduce reactive and adaptive planning. El Makrini et al. [33] used a hierarchical finite-state machine to reassign tasks based on the operator's current workload and physical strain. For real-time adaptation, Zhou et al. [34] developed a linear temporal logic planner that allows robots to respond to local changes using eye-in-hand cameras. Pupa et al. [35] proposed a modular architecture that separates high-level scheduling from low-level trajectory planning to improve safety.

Nevertheless, most existing methods do not verify whether perceived assembly states satisfy the assembly constraints. Without such verification, unexpected human actions or sensing noise can lead planners to operate on outdated or incorrect states, causing errors that propagate into execution and often require manual intervention to resolve.

III. METHODOLOGY

To address the existing gaps, we propose a design-grounded human-aware planning framework for multi-robot structured

TABLE I
DEFINITION OF NOTATION.

Symbol	Description
\mathcal{D}	Design artifact (e.g., CAD, BIM, or PDF)
V	Set of design components
\mathbf{A}	Multidimensional component array extracted from \mathcal{D}
I^{des}	Design image rendered from \mathcal{D}
O_t	RGB-D observation at iteration t , consisting of I_t^{RGB} and I_t^{Depth}
I_t^{RGB}	RGB images at iteration t
I_t^{Depth}	Depth images at iteration t
$\tilde{I}_t^{\text{perc}}$	Design-aligned perceptual representation
U_t^{raw}	Symbolic hypothesis of the uninstalled component set
I_t	Installed component set at iteration t
U_t	Uninstalled component set at iteration t
Γ_{rules}	Rule-based reconciliation operator
\mathcal{R}	Heterogeneous robot team
\mathcal{H}	Set of human collaborators
C_j	Capability profile of robot r_j
T_t	Frontier of admissible components at iteration t
Γ_i^t	Robot assignment for component v_i at iteration t
P_t	Task assignment plan at iteration t
\mathcal{E}_t	Event flag indicating a detected state inconsistency
\mathcal{B}_t^k	Behavior Tree executed by robot r_k at iteration t

assembly. We formalize the planning problem by defining symbolic assembly states, admissible component frontiers, and a minimal-change rule for plan updates under human intervention. The resulting architecture consists of a symbolic state synthesis module and a human-aware planning module. Table I summarizes the notation used in the following sections.

A. Problem Formulation

The structured assembly task is specified by a design artifact \mathcal{D} , which defines the components, their geometric and topological relations, and the required installation order. In practice, the artifact is commonly available in formats such as CAD, BIM, or PDF. Although the file format may differ across domains, the encoded design information is equivalent. During execution, the workspace state changes over time due to robot actions, human interventions, and environmental variation, requiring continuous state updates and replanning.

1) **Entities and inputs:** Let $V = \{v_1, \dots, v_N\}$ denote the set of structural components specified by a design artifact \mathcal{D} . The robotic team is denoted by $\mathcal{R} = \{r_1, \dots, r_K\}$. Each robot r_j is associated with a capability profile C_j , which encodes payload limits, kinematic reach, end-effector type, and workspace constraints. Human collaborators are represented by a set \mathcal{H} of uncontrollable but observable agents.

At iteration t , the system obtains an observation O_t and classifies each component in V as installed or uninstalled, forming I_t and U_t . Changes in these sets reflect both robot execution and possible human intervention. Human interventions are not modeled explicitly and are incorporated only through updates to the perceived state.

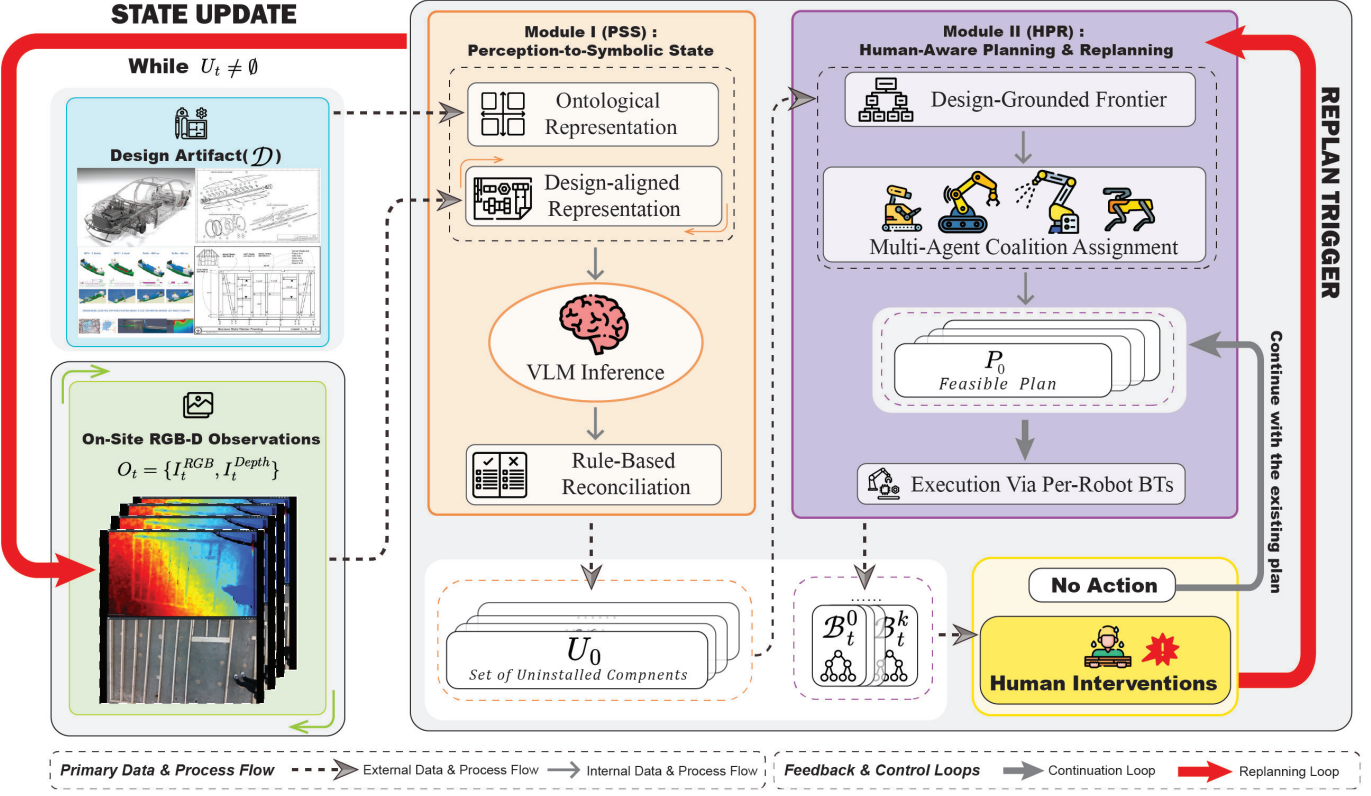


Fig. 1. Overview of the proposed planning framework, showing the interaction between the Perception-to-Symbolic State module and Human-Aware Planning and Replanning module in a closed-loop perception to task planning process.

2) **Problem statement:** Each component $v_i \in V$ is associated with a prerequisite set $Pre(v_i)$ derived from the design artifact \mathcal{D} . The set $Pre(v_i)$ encodes installation precedence relations specified by the design and is assumed to be known.

At planning iteration t , the admissible frontier T_t consists of all uninstalled components whose prerequisites are fully installed according to the verified symbolic state:

$$T_t = \{v_i \in U_t \mid Pre(v_i) \subseteq I_t\}. \quad (1)$$

A plan at iteration t assigns each component in T_t to a feasible robot coalition responsible for its installation. An assignment is feasible only if the selected robots satisfy all capability constraints for the component. These constraints include payload limits, kinematic reach, collision safety, and awareness of perceived human occupancy. All constraints are evaluated using the current observation O_t .

Human-triggered events are detected when changes in the uninstalled set cannot be explained by robot execution. Such discrepancies are recorded as an event flag \mathcal{E}_t , indicating that the current plan may no longer be consistent with the updated state. If no human-triggered event is detected, the previous plan is retained. Otherwise, the planner selects a new feasible plan that minimizes the plan-edit distance $d(P_t, P_{t-1})$:

$$P_t = \begin{cases} P_{t-1}, & \mathcal{E}_t = \text{NONE}, \\ \arg \min_{P_t} d(P_t, P_{t-1}), & \mathcal{E}_t \neq \text{NONE}. \end{cases} \quad (2)$$

A plan P_t specifies, for each admissible component $v_i \in T_t$, a set of robots assigned to install it, denoted by $\Gamma_i^t \subseteq \mathcal{R}$. The

plan-edit distance is defined as the number of components whose assigned robots change between iterations:

$$d(P_t, P_{t-1}) = |\{v_i \in T_t \cap T_{t-1} \mid \Gamma_i^t \neq \Gamma_i^{t-1}\}|. \quad (3)$$

B. Framework architecture

Building on the problem formulation in Sec. III-A, the proposed framework defines a closed-loop architecture for HRC structured assembly. As illustrated in Fig. 1, the architecture integrates the static design specification, live RGB-D observations, and domain knowledge into a unified semantic planning framework that supports adaptive multi-agent coordination.

Module I, Perception-to-Symbolic State (PSS) converts raw perceptual data $O_t = \{I_t^{\text{RGB}}, I_t^{\text{Depth}}\}$ and the design artifact \mathcal{D} into verified symbolic states of the current assembly procedure. It aligns the design geometry with the physical scene, performs VLM-based semantic matching, and applies deterministic rule-based reconciliation to produce the uninstalled component set U_t for downstream planning.

Module II, Human-Aware Planning and Replanning (HPR) takes these symbolic states as input and generates the corresponding multi-robot assembly plan P_t . It identifies the admissible frontier of installable components, determines feasible robot coalitions based on physical capabilities, and compiles the resulting assignments into per-robot behavior trees \mathcal{B}_t^k that support parallel execution and synchronized collaborative actions.

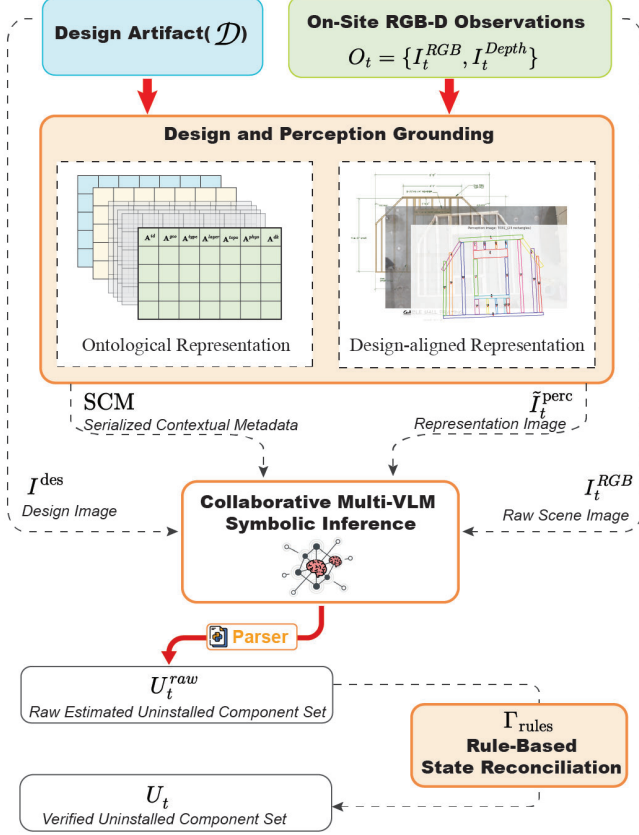


Fig. 2. Overview of the Perception-to-Symbolic State module, which synthesizes a verified symbolic assembly state from design specifications and RGB-D observations..

After each iteration, the PSS module updates the assembly state. If the observed progression matches the expected evolution, the system continues executing the current plan. When human interventions lead to changes in the observed state, the system detects the update and triggers a new planning cycle. Only the parts of the plan affected by the change are refreshed, while the remaining actions continue without interruption.

C. Module I: Perception-to-Symbolic State

As shown in Fig. 2, the PSS module synthesizes verified symbolic assembly states by aligning design specifications with perceptual observations. It first converts the design artifact into a structured ontological array \mathbf{A} that encodes component identity, geometry, dependencies, and assembly rules. From this representation, a design image I^{des} and serialized contextual metadata (SCM) are generated to provide geometric and semantic priors. In parallel, the RGB-D observation O_t is transformed into a design-aligned perceptual image \tilde{I}_t^{perc} .

Given these aligned representations, the multiple VLM-based agents infer a preliminary symbolic hypothesis U_t^{raw} of the uninstalled component set from $(I^{des}, \tilde{I}_t^{perc})$, the SCM, and the RGB image I_t^{RGB} . This hypothesis is then refined by a rule-based reconciliation operator Γ_{rules} , which enforces the structural, semantic, and geometric constraints encoded in \mathbf{A} to produce a deterministic symbolic state U_t . The verified state U_t serves as the input to the planning module.

1) Structured ontological representation:

a) *The design image I^{des}* : To initiate this process, the design artifact is first parsed into its geometric elements. Such elements correspond to the basic drawing entities provided by some commonly used design formats (e.g., line and curve segments in CAD file). The system reconstructs component primitives from these inputs. All structural members are represented in a shared coordinate frame. Using the reconstructed component primitives, the system generates the design image I^{des} , which visualizes the layout of all components in a common coordinate frame. This image defines the reference frame used to align the perceptual representation \tilde{I}_t^{perc} in the VLMs inference stage.

b) *The multidimensional component array \mathbf{A}* : From the same reconstructed primitives, the system constructs the multidimensional component array \mathbf{A} , which provides a unified symbolic representation of the design. Each row represents a component, and each column group encodes a category of design information. As illustrated in Fig. 3, the array is organized into seven parts:

$$\mathbf{A} = [\mathbf{A}^{id} \mid \mathbf{A}^{geo} \mid \mathbf{A}^{type} \mid \mathbf{A}^{layer} \mid \mathbf{A}^{topo} \mid \mathbf{A}^{phys} \mid \mathbf{A}^{dk}].$$

Each sub-array captures a specific aspect of component identity, geometry, semantics, structure, or physical feasibility. Their definitions and functional roles are summarized in Table II. The instantiation of these sub-arrays is further described in Sec. IV-A.

c) *Component array to SCM*: To support the VLMs inference process, \mathbf{A} is converted into the SCM stored in a structured text format such as JSON. The document contains global metadata that records design constants including project identifiers, reference coordinate systems, material standards, and measurement units, and it also contains component-level entries that encode the fields of the seven arrays in \mathbf{A} . This serialized metadata serves as the structured textual input for the VLM-based reasoning module.

This ontological representation, together with the rendered design image and the SCM, encodes design geometry and structural dependencies. It defines the geometric frame, the component dependencies, and the rule-based constraints that support reliable symbolic reasoning in next planning stages.

2) *Design-aligned perceptual representation*: With the design image and the structured component array establishing

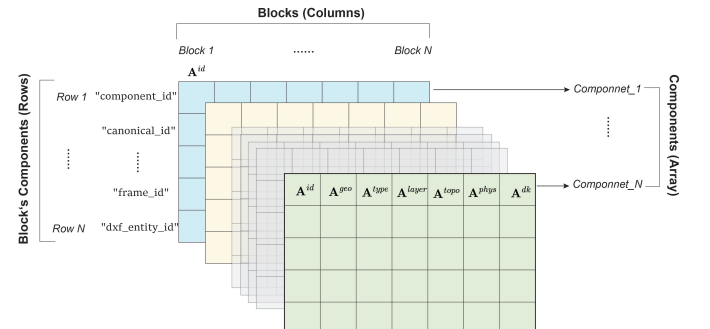


Fig. 3. Structure of the multidimensional component array \mathbf{A} .

TABLE II
DEFINITION AND FUNCTIONAL ROLES OF THE COMPONENT ARRAY \mathbf{A} .

Sub-array	Definition	Functional Role
\mathbf{A}^{id}	Defines component identifiers and reference keys.	Supports indexing across perception and planning.
\mathbf{A}^{geo}	Defines component geometry (pose, dimensions, bounding box).	Supports design alignment and feasibility checking (e.g., capability and constraint evaluation).
\mathbf{A}^{type}	Defines the functional type of each component.	Constrains interpretation in perception and action selection in planning.
\mathbf{A}^{layer}	Defines layering and grouping relations.	Supports multi-layer reasoning under occlusion.
\mathbf{A}^{topo}	Defines structural relations (adjacency and support).	Supports dependency checking and admissible frontier computation.
\mathbf{A}^{phys}	Defines physical properties (mass and material attributes).	Supports capability-aware task allocation.
\mathbf{A}^{dk}	Defines domain knowledge and assembly rules.	Guides state reconciliation and enforces valid configurations.

a common reference frame, the RGB-D observation O_t is transformed into a design-aligned geometric abstraction $\tilde{I}_t^{\text{perc}}$ through multimodal segmentation, primitive extraction, and topology-aware refinement, which is illustrated in Fig. 4.

a) **Multimodal scene segmentation:** The segmentation stage extracts structural regions from the RGB-D observation O_t by suppressing background content. The RGB image first undergoes background suppression to reduce interference from non-structural objects and illumination variation. It is then converted into the CIE-Lab color space to improve robustness under varying lighting conditions. Each pixel is embedded into a feature vector that combines its color channels, normalized depth, and normalized spatial coordinates. This multimodal feature space captures photometric and geometric cues relevant to structural material. A clustering procedure partitions the feature space into coherent regions, and the region consistent with expected material appearance and depth characteristics is selected as the candidate assembly region.

Within this region, a morphological gradient operator [36] enhances material boundaries, and an edge detector converts these transitions into an edge set that suppresses background clutter. This segmentation result forms a geometric basis for the subsequent primitive extraction stage.

b) **Geometric primitive extraction:** The extracted edge set is transformed into a structured representation of geometric primitives that approximate the visible components. The Probabilistic Hough Transform [37] aggregates distributed edge information into a compact set of line hypotheses. Hypotheses that are nearly collinear or overlapping are merged to reduce fragmentation, and the resulting lines are grouped by dominant orientation and spatial proximity. For each group, a minimum-area bounding primitive is estimated to form an initial geometry set. This set reflects specific component shapes and provides a link between raw edges and structural inference.

c) **Topology-aware refinement:** The initial geometry set is refined through checks that enforce geometric regularity and structural topology. First, geometric primitives that correspond to a single design element are merged when detection errors cause them to appear as multiple fragments. Conversely, when

a primitive spans multiple component adjacencies specified in the design, it is subdivided to recover the intended component boundaries and spatial relationships.

Next, a geometric filtering step removes primitives whose shape or scale violates geometric constraints derived from the design representation. This step suppresses spurious detections caused by background textures or depth noise. Temporal consistency is enforced by comparing each primitive with its corresponding instance from the previous time step. This comparison reduces inter-frame jitter and preserves stable geometric identity across the RGB-D sequence. The refinement process produces a coherent and topologically consistent geometric representation, which serves as the design-aligned perceptual image $\tilde{I}_t^{\text{perc}}$.

By transforming raw RGB-D observations into a design-aligned perceptual representation, this refinement process yields a structured geometric input suitable for downstream

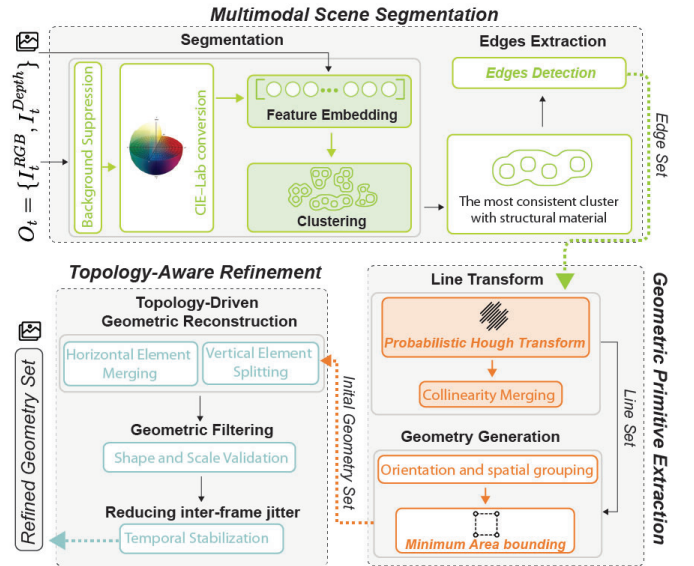


Fig. 4. Design-aligned perceptual representation pipeline for converting raw RGB-D observations into structured geometric primitives.

symbolic reasoning. Implementation details specific to the case study are provided in Section IV-B.

3) **VLM-based symbolic inference:** The VLM-based inference stage compares the design image with the design-aligned perceptual representation to determine which components are installed and which remain uninstalled. To ensure reliable matching, the system uses a structured prompting strategy that provides explicit context descriptions, standardized templates, and a fixed output format [38]. The prompt instructs the model to analyze the detected geometric primitives in \hat{I}_t^{perc} and to associate them with the corresponding components in I_t^{des} under the constraints encoded in the SCM. An additional RGB image I_t^{RGB} is used to support the removal of non-structural detections through a supplementary filtering prompt.

The prompting strategy uses Chain-of-Thought [39] to structure the reasoning process. The model filters perceptual noise and performs hierarchical component matching under geometric and topological constraints. After the matching geometric assignments are made, the model checks the topological relations to confirm that each component satisfies the required connections and ordering rules. The procedure also applies dependency-based inference, where the model infers missing components when their supporting elements are detected, and no conflicting evidence is present.

This stage output is the initial uninstalled set U_t^{raw} , which contains component-level match decisions and possible inference labels. This set is then refined by a deterministic reconciliation operator that enforces structural constraints to correct missing assignments and removes inconsistent matches.

4) **Rule-based state reconciliation:** The final stage of the state synthesis approach refines the initial hypothesis U_t^{raw} , obtained from VLM-based perceptual inference, into the verified symbolic state. This process is carried out by the reconciliation operator Γ_{rules} . The operator applies the structural relations in \mathbf{A}^{topo} , the rule-based constraints in \mathbf{A}^{dk} , and the geometric information in \mathbf{A}^{geo} to ensure that the symbolic states satisfy all structured constraints.

The operator applies two steps. The first step adds components that must be present for the detected structure to be valid. When the model identifies an element whose installation requires specific supporting components, the missing supports are inserted if no conflicting evidence is observed. The second step removes components whose inclusion would violate the dependency rules or structural relations encoded in the design. Elements are removed when they appear without their required predecessors or when their inferred placement contradicts the structural layout. These two steps are applied iteratively until no additional updates are needed, producing the verified uninstalled set U_t .

D. Module II: Human-Aware Planning and Replanning

The HPR module updates and executes task assignments within the closed-loop procedure in Algorithm 1. At each iteration t , it computes the admissible frontier T_t from the current symbolic state (I_t, U_t) , updates the task assignment plan P_t by preserving unchanged assignments and allocating remaining admissible tasks under feasibility constraints, and updates per-robot behavior trees \mathcal{B}_t^k for execution.

Algorithm 1 Reactive Closed-Loop Planning and Execution

Require: design artifact \mathcal{D} , component array \mathbf{A} , robot team

```

 $\mathcal{R}$ 
1:  $t \leftarrow 0; P_{-1} \leftarrow \emptyset; U_{-1} \leftarrow V$ 
2: while  $U_{t-1} \neq \emptyset$  do
3:   State Update
4:    $O_t \leftarrow \text{PERCEIVE}(t)$ 
5:    $U_t^{\text{raw}} \leftarrow \text{PSS}(\mathcal{D}, \mathbf{A}, O_t)$ 
6:    $U_t \leftarrow \Gamma_{\text{rules}}(U_t^{\text{raw}}, \mathcal{D}, \mathbf{A})$ 
7:    $I_t \leftarrow V \setminus U_t$ 
8:    $\mathcal{E}_t \leftarrow \text{DETECTEVENT}(U_{t-1}, U_t, P_{t-1})$ 
9:   Frontier Evaluation
10:   $T_t \leftarrow \text{FRONTIER}(U_t, \mathcal{D})$ 
11:  Plan Update
12:  if  $\mathcal{E}_t = \text{NONE}$  then
13:     $P_t \leftarrow P_{t-1}$ 
14:  else
15:    Preserve valid assignments from  $P_{t-1}$  for tasks in  $T_t$ 
16:     $P_t \leftarrow \text{assign remaining admissible tasks in } T_t \text{ to } \mathcal{R}$ 
17:  end if
18:  BT Update and Execution
19:  for each  $r_k \in \mathcal{R}$  do
20:     $\mathcal{B}_t^k \leftarrow \text{BT\_UPDATE}(\mathcal{B}_{t-1}^k, P_{t-1}, P_t)$ 
21:  end for
22:   $\text{TICKBT\_EXECUTOR}(\{\mathcal{B}_t^k\})$ 
23:   $t \leftarrow t + 1$ 
24: end while
25: return  $P_{t-1}$ 

```

1) **Human-aware replanning:** Human intervention here is modeled as a replanning event \mathcal{E}_t . It is detected by comparing the updated uninstalled set U_t with the expected outcome of the previous robot execution. If no event is detected, the existing plan is retained. Otherwise, the planner selects a new feasible assignment that minimally deviates from the previous one, according to the minimal-change rule in (2) and the plan-edit distance in (3). The resulting assignment is executed by the robots, and execution outcomes are fed back to the loop until all components are installed.

2) **Frontier evaluation and feasibility assessment:** Given the current uninstalled set U_t , the planner identifies the admissible frontier T_t of components whose design prerequisites are satisfied. For each frontier component, the planner evaluates feasible robot assignments under the current observation. Feasibility is determined by the robot capability profiles C_j , including payload limits, kinematic reach, collision safety, and perceived human occupancy regions.

3) **Minimal-change task reassignment:** Replanning is triggered only when a human-induced or unexpected state change is detected. When replanning is required, the planner updates the task assignment by approximately minimizing the plan-edit distance $d(P_t, P_{t-1})$. Assignments from the previous planning cycle associated with components that remain admissible under the updated symbolic state are retained. Admissibility here requires that structural prerequisites remain satisfied despite human intervention, which avoids unnecessary increases in the plan-edit distance. Components that are not preserved from

the previous assignment are selected for reassignment. This set includes components that become newly admissible due to state changes and components whose prior assignments are no longer feasible. For these components, the planner performs task allocation using a workload-based heuristic while enforcing the defined feasibility constraints.

4) **Behavior tree generation and update:** The updated task assignment is projected onto robot-specific behavior trees. For each robot r_k , execution is represented by a behavior tree \mathcal{B}_t^k . Tasks whose assignments are unchanged preserve their corresponding subtrees in \mathcal{B}_{t-1}^k . Only reassigned components generate new or modified subtrees in \mathcal{B}_t^k . Single-robot tasks are mapped to sequential execution structures. Tasks requiring multiple robots include synchronization nodes that enforce coordinated execution across the corresponding trees. Behavior trees are executed asynchronously to allow parallel execution.

IV. CASE STUDY

The proposed framework is validated on a real 27-component timber frame wall assembly task. Fig. 5 depicts the real assembly setup, while the complete timber-frame design is shown in Fig. 6 (right side). Two collaborative robots operate on opposite sides of the workcell, and an overhead RGB-D camera provides a registered top-down view.

The timber-frame wall is a representative structured assembly task with geometric similarity across members and strict prerequisite relations. These properties create ambiguous matches under clutter and occlusion. The frame also contains components with different physical properties and functional roles. These include short studs that can be handled by a single robot and long plates that require cooperative handling. Human workers may install or remove any component at unscripted times. These actions introduce sudden changes in the uninstalled set, alter feasible coalitions, and create conflicts with ongoing robot tasks. The combination of these factors creates a realistic environment that supports a comprehensive evaluation of the robustness of our method.

A. Ontological representation of the DXF design file

The elevation drawing of this wall is available in Drawing Exchange Format (DXF) format and serves as the design

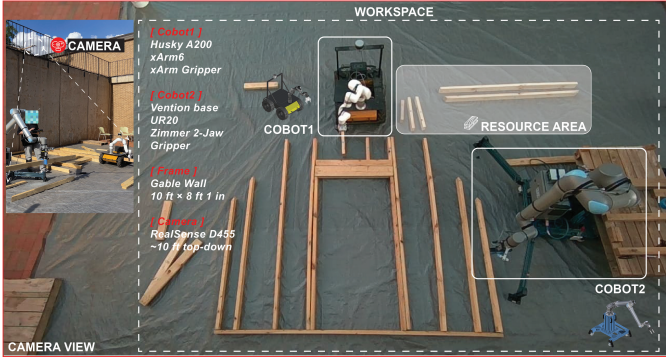


Fig. 5. Example layout used for the case study. The configuration includes two heterogeneous collaborative robots, an overhead RGB-D camera, and the design coordinate frame registered to the workspace.

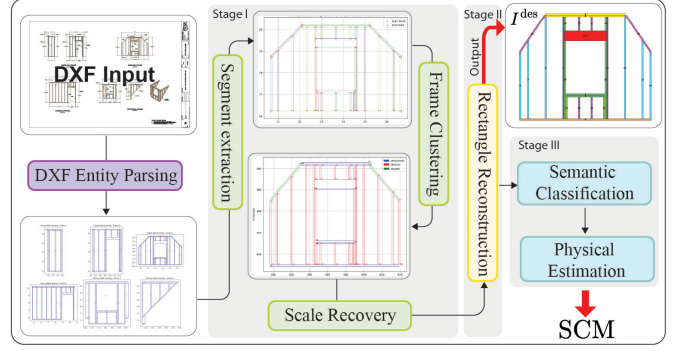


Fig. 6. Pipeline for generating the ontological representation.

artifact for constructing the ontological representation. The processing workflow, illustrated in Fig. 6, begins by decomposing the DXF file into its elementary CAD entities, including LINE and LWPOLYLINE. Each polyline is subdivided into its constituent segments, producing a detailed geometric description of the drawing. These segments form the primitive units from which the structural layout is recovered. To recover the structural layout, segments are grouped into coherent component clusters based on spatial adjacency, supported by a reading-order prior that follows the typical top-to-bottom, left-to-right organization of architectural drawings.

To ensure metric consistency, we recover scale by mapping DXF units to physical dimensions, assigning the shortest detected segment to the nominal lumber thickness of 1.5 inches. All geometric quantities are then expressed in real-world units. Rectangular component candidates are reconstructed by pairing parallel and nearly equal-length line segments separated by referring to the nominal lumber thickness. This procedure yields the horizontal, vertical, and diagonal rectangles that form the geometric footprint of the timber members.

Using these reconstructed rectangles, the design image I^{des} is rendered in the unified coordinate frame, where each rectangle is drawn with its detected geometry and assigned a fixed color that denotes its construction role (e.g., plates in yellow, headers in red, studs in cyan). These color encodings serve as semantic cues that guide VLM-based matching by disambiguating component types during visual reasoning. The resulting image provides the geometric and spatial reference used during VLMs reasoning. The same rectangles are used to instantiate the \mathbf{A} , from which the SCM file is serialized in JSON format. Fig. 7 illustrates the global metadata and the seven array fields for a representative component (window_1_header_layer_1).

This example demonstrates how the abstract representation introduced in Sec. III-C1 is instantiated for a real assembly task. In this example, the identity array \mathbf{A}^{id} specifies the component identifier, canonical name, opening association, and the originating DXF entity. The geometry array \mathbf{A}^{geo} explicitly records rectangle pose and dimensions, including its center coordinates, length, width, orientation, and bounding box in design units. Semantic role information is instantiated in \mathbf{A}^{type} by labeling the component as a window header, while \mathbf{A}^{layer} indicates its membership in a multi-layer group

<pre>"frame_metadata": { "frame_id": "Gable Wall Framing - Frame 1", "units": "inch" }, "construction_constants": { "material_profile_standard": "2x6", "lumber_thickness_in": 1.5, "tolerance": {"len_in": 0.5, "pos_in": 0.75, "angle_deg": 3.0}, "gap_tolerance_in": 0.25, }, </pre>	<pre>"A_topo": { "adjacent_to": ["window_1_king_stud_left", "window_1_trimmer_left_down", "window_1_trimmer_left_up", "window_1_cripple_up_1", "window_1_cripple_up_2", "window_1_trimmer_right_up", "window_1_trimmer_right_down", "window_1_king_stud_right", "window_1_header_layer_2"], "predecessors": ["window_1_king_stud_left", "window_1_trimmer_left_down", "window_1_trimmer_right_down", "window_1_king_stud_right"], }, </pre>
<pre>"A_id": { "component_id": "window_1_header_layer_1", "canonical_id": "GW_F1_HEADER_W1", "role": "header", "opening": "W1", "index": 0, "frame_id": "Gable Wall Framing - Frame 1", "design_type": "DXF", "dxf_entity_id": "rect_003", }, </pre>	\mathbf{A}^{topo}
<pre>"A_geo": { "center_xy_in": [567.8068, 465.1600], "rotation_deg": 0.0, "length_in": 38.5, "width_in": 9.25, "thickness_in": 1.5, "bbox_in": { "xmin": 548.5568, "xmax": 587.0568, "ymin": 460.5350, "ymax": 469.7850 }, }, </pre>	\mathbf{A}^{phys}
<pre>"A_dk": { "rules": ["header must span opening; needs king stud and trimmers", ] }, </pre>	\mathbf{A}^{type}
	\mathbf{A}^{layer}

Fig. 7. Representative example of the arrays in \mathbf{A} for the component `window_1_header_layer_1`.

through a shared group identifier. The topological array \mathbf{A}^{topo} lists adjacent and predecessor components. Physical properties such as the estimated mass are stored in \mathbf{A}^{phys} and later used for capability-aware task allocation. Finally, \mathbf{A}^{dk} encodes construction-specific assembly rules that enable deterministic reconciliation under ambiguous perceptual observations.

B. Design-aligned representation of real-site RGB-D images

This section instantiates the design-aligned perceptual representation in Sec. III-C2 for real-site RGB-D data. Two representative settings were evaluated: *indoor* and *outdoor*. Indoor data were captured using an Intel RealSense D435, while outdoor data used a RealSense D455, whose global shutter improves depth stability in strong illumination. Both are at a resolution of 1280×720 , using the camera's built-in intrinsic parameters for metric projection.

Indoor data were collected in a confined workspace with artificial lighting. Although the illumination remained stable, the limited space led to unavoidable clutter around the wall frame, and the floor surface introduced background edges and texture noise. Outdoor data were recorded in an open area using a single-color tarp as the background. This setup removed clutter almost entirely but introduced natural light variability due to sunlight reflections, cloud cover, and moving shadows. Example images are shown in Fig. 8.

Following the procedure outlined in Sec. III-C2, the RGB-D observations are conditioned to extract structural regions and suppress background interference. Although the segmentation follows a common sequence, the relative weighting of appearance and depth cues differs between indoor and outdoor settings due to their sensing characteristics. For indoor scenes, depth is stable under uniform lighting, but clutter and floor texture introduce background edges. We therefore apply



Fig. 8. Example images from the different environmental conditions.

background suppression and hole filling before clustering. Background regions are removed, small distractions are filled, and each pixel is embedded in a six-dimensional feature vector

$$[L, a, b, w_x x, w_y y, w_z z],$$

where (L, a, b) denote pixel color in the CIELAB color space, (x, y) are normalized image coordinates, and z is normalized depth. The weights w_x , w_y , and w_z balance appearance, spatial proximity, and depth cues. They are empirically selected per setting and kept fixed across all experiments. The K-means clustering [40] algorithm is used to group the pixels into coherent regions, and a scoring rule selects the cluster that best matches the expected structural geometry by scoring from color, depth, and the pixels coordination. For outdoor scenes, the segmentation assigns a higher weight to depth cues than to appearance cues. Pixels with inconsistent depth are filtered out, and the resulting depth mask restricts the clustering stage to regions more likely to contain structural elements.

After segmentation, a morphological gradient [36] highlights the component boundaries, and the Canny detector [41] converts these boundaries into edge maps used for geometric processing. Fig. 9 shows representative results for both indoor and outdoor settings, including masked RGB images after the background suppression step, the segmentation mask result, and the raw Canny edges.

The filtered edges are converted into geometric elements in this stage. Local edge patterns are aggregated into line segments using the Probabilistic Hough Transform (PHT) [37]. Segments that lie along nearly the same direction are merged, then grouped according to their main orientation and location. Because timber-frame structures are rectilinear, each group is converted to a rectangle based on the Freeman and Shapira [42]'s minimum-area bounding theory. This produces

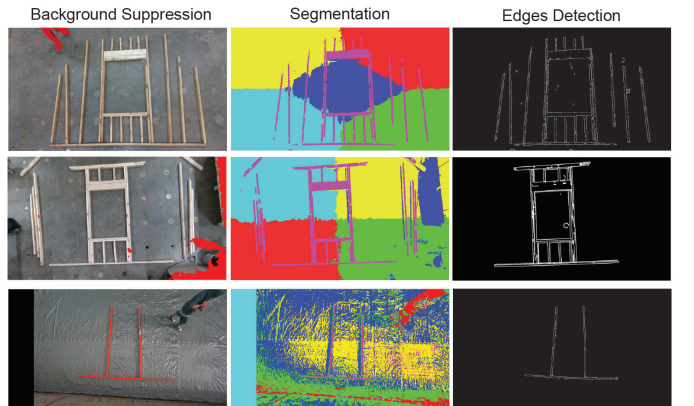


Fig. 9. Multimodal segmentation results in indoor and outdoor conditions.

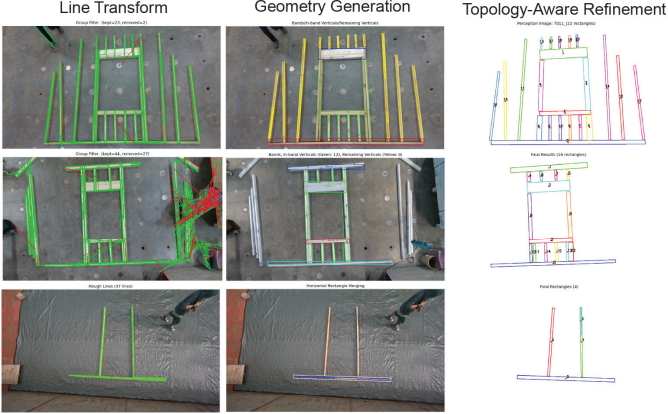


Fig. 10. Geometric primitive extraction and rectangle reconstruction.

an initial set of rectangles that outline candidate structural components.

The initial rectangles are further adjusted to align with the structure of the wall frame. Long horizontal members are merged if they appear fragmented. Vertical elements that cross these horizontals are divided at the intersection to recover the correct structural layout. Rectangles that are clearly too stretched, too short, or inconsistent in scale are removed through common geometric checks. Finally, each rectangle is compared with its counterpart in the previous frames, which reduces flicker caused by depth noise, glare, or temporary occlusions from people passing through the scene. Fig. 10 shows representative outputs, including lines set, geometric groupings, and the final rectangle set.

The final output is a clean set of design-aligned rectangles that summarize the visible structure. This representation is then passed to the VLMs reasoning stage with other outputs in the ontological representation procedure.

C. VLM-based semantic inference in real scenes

Fig. 11 shows the VLM-based semantic inference workflow used in the case study. The workflow employs two VLM-based reasoning agents that operate on the same design-aligned perceptual representation. A Match Agent performs semantic inference grounded in the design specification by aligning perceptual primitives with the design ground truth. In parallel, a Filter Agent evaluates scene consistency by identifying perceptual primitives that are geometrically or visually inconsistent with the observed scene. The outputs of both agents are jointly evaluated by a deterministic reconciliation operator, which produces the final verified uninstalled set. Representative reasoning examples and the exact prompts used by the VLM agents are provided in Appendix A. The following paragraphs describe how this process operates under real-site sensing.

The Match Agent receives the design image, the design-aligned perceptual representation, and the SCM in a shared coordinate frame. The agent is guided through a series of reasoning steps aligned with construction knowledge. The matching procedure begins with elements that are easiest to locate. For example, long horizontal members are identified first because they outline the wall and set clear positional limits

for other parts. Once these boundaries are recognized, the model determines the geometry of the opening, including its sill, header, and surrounding spans. The agent then resolves the major vertical components near the opening by checking their layout relative to the established boundaries. Studs across the frame are interpreted next with attention to spacing, alignment, and the type rules encoded in the SCM. Diagonal elements are resolved last by evaluating their orientation and attachment relations. Finally, a verification step compares the inferred configuration with structured constraints.

For the Filter Agent, it evaluates perceptual consistency by removing geometric primitives that do not correspond to visible structural members. It operates on the same design-aligned perceptual representation and RGB image. In uncluttered scenes, this process preserves the original perceptual set. In cluttered scenes, it suppresses spurious detections caused by background objects, temporary occlusions, or depth artifacts.

In practice, both agents output their reasoning results in a structured JSON format. The Match Agent reports, for each design component, its predicted installation status, matched perceptual primitive, and a brief justification. The Filter Agent returns the subset of perceptual primitives consistent with the observed scene. These outputs are combined during reconciliation to produce the verified uninstalled set.

The raw semantic hypothesis may still contain inconsistencies due to occlusion, clutter, or reasoning errors. A deterministic reconciliation operator is used to evaluate these hypotheses against structural and topological rules. The module applies three rule-based enforcement steps that reflect basic requirements of the timber-frame design. These steps include support dependency completion, structural consistency pruning, and adjacency refinement. Support dependency completion ensures that a component is included only when all necessary supporting members are present and when the corresponding perceptual primitives are retained by the Filter Agent. Structural consistency pruning removes components whose inferred placement contradicts the ordering or geometric relations prescribed by the design. Adjacency refinement revisits the local spatial neighborhood, adding missing elements or removing those that do not exhibit valid support patterns.

These operations address common VLMs failure cases. For example, horizontal members inferred without their supporting studs are removed, short vertical elements near the opening are reinstated when omitted due to partial occlusion, and isolated studs in cluttered areas are eliminated because they do not fit valid structural patterns. After these operations, a verified uninstalled component set is obtained.

D. Planning instantiation for timber frame task

Following the closed-loop planning process described in Sec. III-D, we instantiate the planner by grounding frontier evaluation and capability constraints in the component arrays. In this scenario, feasibility is determined solely by payload capacity. Component masses are obtained from the physical attribute array A^{phys} . A robot team is feasible for a component if its combined payload capacity exceeds the component mass.

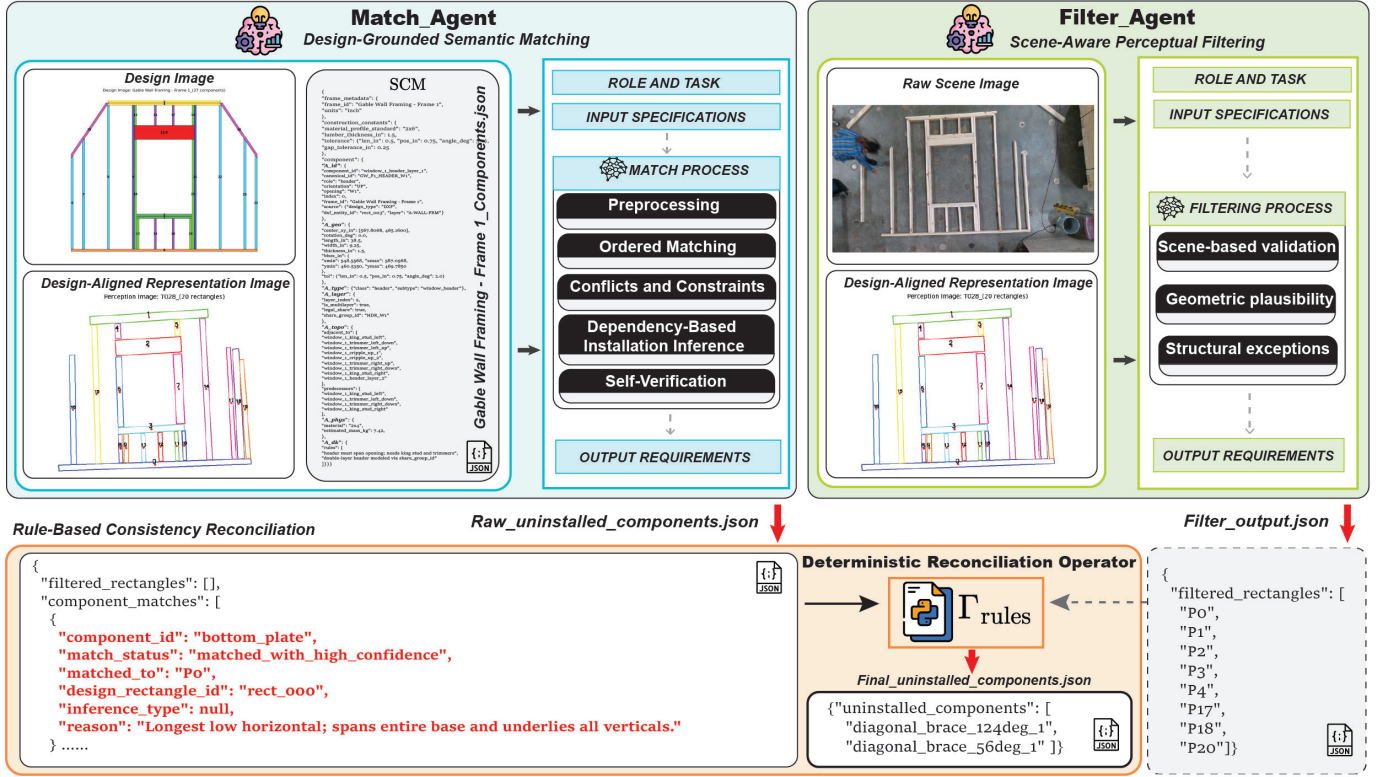


Fig. 11. VLM-based symbolic inference workflow, illustrating the interaction between the Match Agent, the Filter Agent, and rule-based consistency reconciliation.

The admissible frontier is derived from prerequisite relations encoded in the design knowledge array A^{dk} . For example, bottom plates must be installed before studs. Studs adjacent to openings must be installed before headers. Components above an opening become admissible only after their supporting studs are complete. The frontier order produced during planning follows directly from these domain rules.

Heterogeneous payload capacities, together with the minimal-change update, allow task assignments to remain consistent across planning cycles. Robots that remain feasible for a component retain their assignments. Components that become newly admissible are assigned to feasible robots with lower current workload. Human interventions are modeled as installing or removing components. Such actions modify the uninstalled set and may introduce newly admissible components or invalidate existing assignments. In these cases, only the affected components are reassigned, while all other assignments remain unchanged.

The resulting coalitions are directly mapped to robot behavior tree execution structures. Fig. 12 illustrates three representative subtrees generated in this case. For cooperative coalitions, each robot receives a parallel branch containing a shared synchronization node. Robots execute their MOVE and Co-PICK actions independently and wait at the synchronization point until all coalition members are ready. The group then proceeds to a joint CO-INSTALL action, ensuring coordinated placement of heavier components. Single-robot coalitions yield linear MOVE-PICK-INSTALL subtrees without synchronization. Robots remain idle when no component in

the current frontier is assigned to them.

Changes in component admissibility and task reassignment under human intervention are visualized in the execution trace in Fig. 13. For example, the replanning scenario shown in the lower-right panel of Fig. 13 demonstrates a human-triggered plan update during execution. In the original plan execution, the planner assigns Cobot 1 to install window_1_trimmer_right_up, while Cobot 2 executes a pick action for stud_5, both of which are admissible at that iteration. In the next iteration, a human installs window_1_cripple_up_2 ahead of the planned sequence. This action introduces a discrepancy between the expected and observed installation states, which is detected by the state update module and triggers a replanning event. Following the minimal-change update rule, only the assignments affected by this discrepancy are revised.



Fig. 12. Representative behavior tree structures for single-robot and cooperative installation tasks.

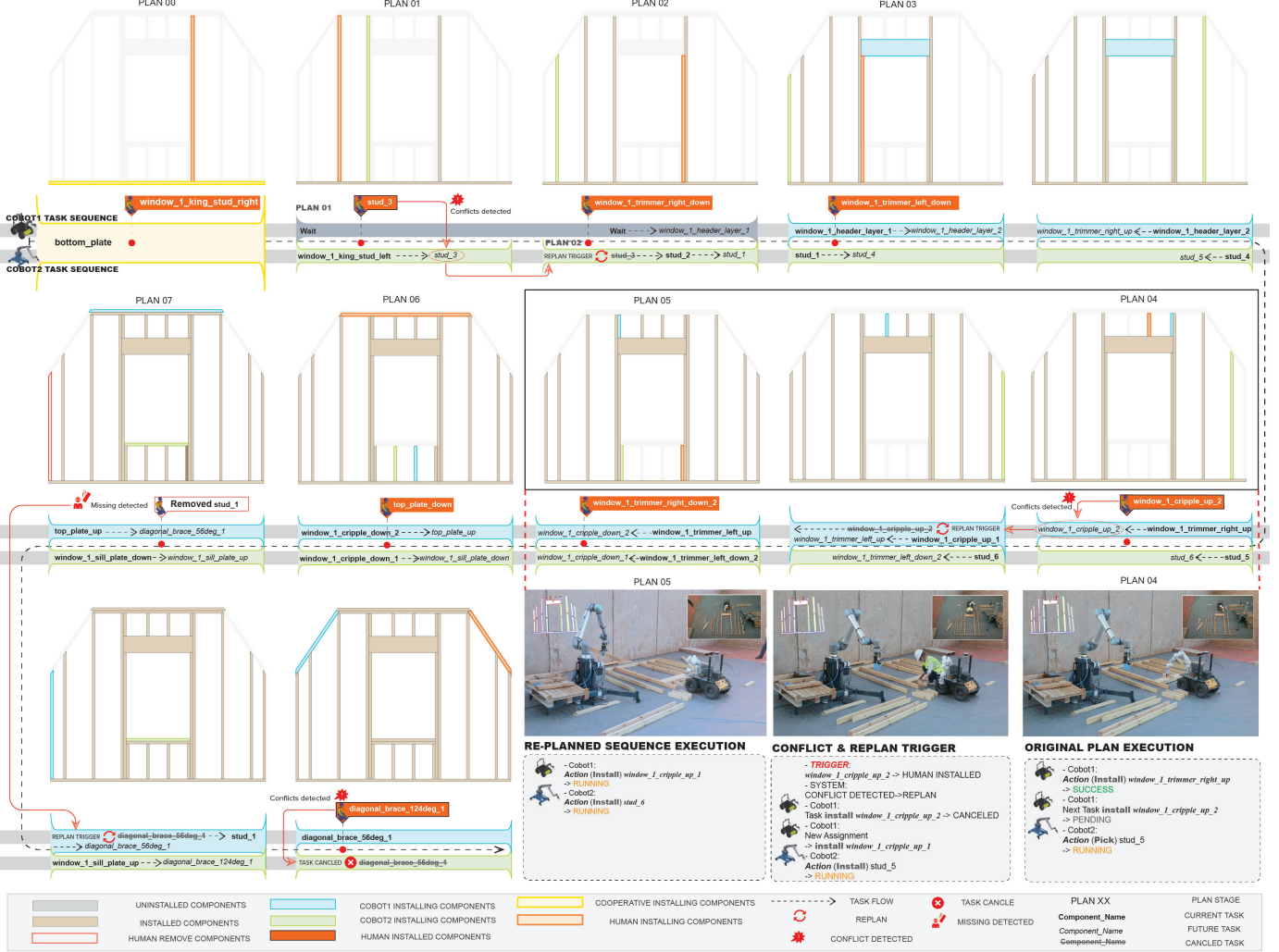


Fig. 13. Closed-loop execution trace of the full timber-frame wall assembly, illustrating task progression and replanning events.

The task associated with `window_1_cripple_up_2` is canceled, while unaffected assignments are preserved. In the re-planned execution, Cobot 1 is reassigned to install `window_1_cripple_up_1`, whereas Cobot 2 continues its previously assigned task without interruption.

E. Quantitative evaluation and results

This section evaluates the two core components of the proposed framework. The first experiment assesses whether the PSS module can convert real RGB-D observations into symbolic states suitable for task planning. The second experiment evaluates the planning system in a task-level planning simulation without physical execution, focusing on payload-aware allocation and plan adaptation under human intervention. Detailed experimental settings and results are reported in the following subsections.

1) *VLMs semantic inference evaluation*: The evaluation dataset comprises 300 RGB-D images (200 indoor, 100 outdoor). The indoor dataset contains both uncluttered scenes and cluttered scenes. In the uncluttered scenes, only structural components are visible, whereas the cluttered scenes include

additional objects such as tools, materials, or human presence that partially occlude the frame. These scene conditions reflect common situations encountered during on-site construction.

We evaluate the PSS module using three representative and affordable VLMs: GPT-5, Gemini-3-Pro, and Claude-Opus-4.5. Each model is used as a reasoning backend under three input configurations.

Baseline (Base), which compares the raw RGB scene image with the design image; *Design-Grounded Matching* (M), which applies design-grounded semantic matching using a single VLM agent; and *Design-Grounded Matching with Filtering* (M+F), which augments design-grounded matching with a parallel VLM-based consistency filtering agent.

Model accuracy is computed as the percentage of correctly identified uninstalled components relative to the ground truth. Table III reports the accuracy of each model under the three input configurations.

2) *Planning Evaluation*: All robots execute tasks using a fixed *Pick–Move–Install* behavior tree. Component masses are obtained from the design artifact and encoded in the physical attribute array, ranging from 1.5 kg for cripple studs to 13.86

TABLE III
VLMs INFERENCE ACCURACY UNDER DIFFERENT CONFIGURATIONS.

Model	Indoor			Outdoor		
	Base	M	M+F	Base	M	M+F
GPT-5	52%	92%	97%	49%	83%	83%
Gemini-3-Pro	44%	78%	86%	61%	48%	48%
Claude-Opus-4.5	23%	56%	62%	28%	34%	34%

kg for the bottom plate. Mass values are computed from the reconstructed component dimensions and standard lumber material properties encoded in \mathbf{A}^{phys} . These values are used directly by the capability predicate defined in Sec. III-A.

To evaluate capability-aware allocation, three representative robot team configurations C_j are considered. The *Homogeneous Team* consists of two robots with identical payload capacities of 11.0 kg, which approximates the handling capability of standard collaborative manipulators commonly used for single-member installation tasks. The *Heterogeneous Team* consists of two robots with payload capacities of 15.0 kg and 6.0 kg, reflecting asymmetric teams where one robot is capable of handling heavier structural components while the other is restricted to lighter elements. In this setting, the lower-capacity robot cannot individually handle heavier components. The *Scalable Team* extends the homogeneous setting by adding a third robot, with all robots assigned a payload capacity of 9.0 kg. This configuration reflects practical upper bounds in on-site HRC assembly. [43] Coordinating more than three robots around a single structural subassembly is uncommon due to workspace constraints and safety considerations [44].

Human interaction is modeled using three policies. The *No-Intervention Policy* assumes that all component state changes result solely from robot execution. The *Random Policy* introduces installation or removal events at unpredictable times. The *Adversarial Policy* removes components that affect structural support and prerequisite satisfaction. The *Cooperative Policy* installs admissible components when possible, emulating collaborative human assistance. Seven scenarios are constructed by combining robot team configurations with human policies. These scenarios are summarized in Table IV.

Four metrics summarize planning performance. The number of execution cycles reports the closed-loop iterations required to complete the assembly. Execution time reports the average computation cost per planning iteration, excluding low-level motion planning and control execution. The plan edit distance,

defined in Sec. III-A, is evaluated over replanning iterations only. Let n_r denote the number of replanning iterations, i.e., iterations for which $\mathcal{E}_t \neq \text{NONE}$. The reported edit distance is computed as

$$\bar{d} = \frac{1}{n_r} \sum_{t=1}^{n_r} d(P_t, P_{t-1}). \quad (4)$$

A value of zero indicates no task reassignment, while larger values indicate more frequent reassignment. The workload deviation measures the balance of task allocation across robots. Let n_j^t denote the number of components assigned to robot r_j at iteration t . And Let $\bar{n}^t = \frac{1}{|\mathcal{R}|} \sum_{r_j \in \mathcal{R}} n_j^t$ denote the average workload at iteration t . The workload deviation is computed as

$$\sigma_n^t = \sqrt{\frac{1}{|\mathcal{R}|} \sum_{r_j \in \mathcal{R}} (n_j^t - \bar{n}^t)^2}. \quad (5)$$

Reported values correspond to the average deviation over all planning iterations. Lower values indicate more balanced allocation, while higher values reflect imbalance due to asymmetric robot capabilities or cooperative installation requirements.

Table V reports results for all scenarios. Further interpretation and discussion of these results appear in Sec. V.

TABLE V
PLANNING PERFORMANCE AND STABILITY RESULTS FOR ALL SCENARIOS.

ID	Cycles	Time (ms)	Edit Distance	Workload Deviation
S1	51.0	0.00	0.000	1.41
S2	37.8	0.03	0.000	0.90
S3	44.9	0.03	0.000	6.33
S4	36.5	0.04	0.000	2.01
S5	105.4	0.03	0.000	3.55
S6	127.6	0.03	0.677	1.22
S7	34.5	0.04	0.000	0.80

V. DISCUSSION

Across all evaluated scenarios, the proposed framework operates robustly in dynamic timber-frame assembly tasks, manages heterogeneous robot coordination, and unscripted human interventions. This performance is substantiated by two key experimental observations.

The evaluation results of the proposed PSS module show that replacing the original scene image with a design-aligned representation helps the VLMs make more accurate and consistent decisions. As shown in Table III, using the design-aligned representation instead of raw RGB images as VLM input improves GPT-5 correctness from 52% to 92% in indoor environments. Furthermore, the filtering agent pushes correctness to 97% by suppressing spurious perceptual primitives introduced by background clutter and partial occlusion. This improvement indicates that abstracting raw visual data into structured geometric primitives reduces the impact of background clutter and floor textures that often introduce misleading edges in raw images. In outdoor environments, design-grounded matching achieves 83% correctness for GPT-5, compared to 49% for the raw RGB baseline, indicating robustness to lighting variation. Adding the filtering agent

TABLE IV
SCENARIO CONFIGURATIONS USED IN THE PLANNING EVALUATION.

ID	Robot Team	Human Policy	Method
S1	Homogeneous	No-Intervention	HPR
S2	Homogeneous	Random	HPR
S3	Heterogeneous	Random	HPR
S4	Scalable Team	Random	HPR
S5	Homogeneous	Adversarial	HPR
S6	Homogeneous	Adversarial	Full Replanning
S7	Homogeneous	Cooperative	HPR

yields no further improvement in this setting, as the background is clean and the filtering step preserves all primitives without removing valid structural elements. These results indicate that the filtering agent improves robustness in cluttered scenes without degrading performance. All results show that the proposed PSS module produces symbolic states that are reliable enough for downstream task planning.

The planning evaluation highlights that precise modeling of robot physical constraints and accurate symbolic states are useful to maintain task feasibility. As shown in Table V, in the heterogeneous team scenario S2, the planner correctly assigns heavier components to the robot with higher payload capacity, while lighter components are distributed across the remaining agents. This allocation achieved a balanced workload distribution of 0.90 despite the asymmetry in robot capacities. Moreover, a direct comparison of adversarial scenarios S5 and S6 validates the robustness of the minimal-change rule. While the full replanning baseline in Scenario S6 suffered from high plan instability with a mean edit distance of 0.677, our approach in Scenario S5 maintained a zero plan edit distance despite repeated human component removals. This contrast shows that the edit-distance objective successfully isolates the impact of local disturbances, allowing unaffected tasks to continue without reassignment. This led to the preservation of workflow continuity, avoiding frequent task switching.

Despite the robust performance demonstrated in the experiments, the current framework has several limitations. For example, under the sensing assumptions adopted in this study, the single-camera configuration was sufficient for the evaluated assembly tasks. However, more complex site conditions may introduce depth noise or occlusions that require a multi-camera configuration to be adequately resolved. In addition, since continuous human motion modeling and human-robot safety constraints are outside the scope of this study, human interventions are simplified as discrete installation or removal events. These limitations reflect the task-level planning scope of this work and do not affect the validity of the proposed planning framework.

VI. CONCLUSION

In summary, our design-grounded human-aware planning framework addresses robust state estimation and adaptive human-aware planning in dynamic assembly environments. The framework synthesizes verifiable symbolic assembly states from ambiguous RGB-D observations by grounding VLM-based semantic reasoning in design-aligned representations and deterministic rule checks. Our symbolic grounding module provides more reliable symbolic state estimates than raw visual baselines and reduces VLMs hallucination under variable site conditions. These verified symbolic states are continuously updated and used to assess task feasibility during execution. With these state updates, the framework maintains consistent task planning despite unscripted human interventions through the use of a minimal-change replanning strategy. These findings suggest that integrating design priors with reactive symbolic task-level planning provides a practical approach to dependable HRC in structured assembly tasks.

In future work, we aim to reduce reliance on explicitly predefined deterministic rules by exploring foundation models and learning-based approaches for automatic rule induction and generalization across assembly domains. In addition, system robustness in complex and dynamic environments can be further improved by incorporating richer sensing cues, such as multi-view or multi-modal inputs. Finally, the current planning problem formulation can be extended to model human motion beyond discrete interventions and incorporate robotics execution feasibility feedback, moving toward task planning methods that better reflect real-world execution constraints.

ACKNOWLEDGMENT

The authors would like to express their gratitude to the Hi-DARS lab for their invaluable equipment and workspace support during the experiments. The authors would also like to acknowledge the financial support for this research received from the U.S. National Science Foundation (NSF) CMMI 2531678. Any opinions and findings in this paper are those of the authors and do not necessarily represent those of the NSF.

REFERENCES

- [1] T. Bock, “The future of construction automation: Technological disruption and the upcoming ubiquity of robotics,” *Automation in Construction*, vol. 59, pp. 113–121, 2015. [Online]. Available: <https://www.sciencedirect.com/science/article/pii/S092658051500165X>
- [2] B. Siciliano, L. Sciavicco, L. Villani, and G. Oriolo, *Robotics*, ser. Advanced Textbooks in Control and Signal Processing, M. J. Grimble and M. A. Johnson, Eds. London: Springer, 2009.
- [3] A. Ranjan Das and M. Koskinopoulou, “Toward sustainable manufacturing: A review on innovations in robotic assembly and disassembly,” *IEEE Access*, vol. 13, pp. 100 149–100 166, 2025.
- [4] A. Ajoudani, A. M. Zanchettin, S. Ivaldi, A. Albu-Schäffer, K. Kosuge, and O. Khatib, “Progress and prospects of the human–robot collaboration,” *Autonomous Robots*, vol. 42, no. 5, pp. 957–975, Jun. 2018.
- [5] M. Tenorth and M. Beetz, “KnowRob: A knowledge processing infrastructure for cognition-enabled robots,” *The International Journal of Robotics Research*, vol. 32, no. 5, pp. 566–590, Apr. 2013.
- [6] L. Homem de Mello and A. Sanderson, “Representations of mechanical assembly sequences,” *IEEE Transactions on Robotics and Automation*, vol. 7, no. 2, pp. 211–227, Apr. 1991.
- [7] B. P. Gerkey and M. J. Mataric, “A Formal Analysis and Taxonomy of Task Allocation in Multi-Robot Systems,” *The International Journal of Robotics Research*, vol. 23, no. 9, pp. 939–954, Sep. 2004.
- [8] S. Zobov, F. Chervinskii, A. Rybnikov, D. Petrov, and K. Vendidandi, “Auto-assembly: a framework for automated robotic assembly directly from cad,” 2023. [Online]. Available: <https://arxiv.org/abs/2301.02643>
- [9] Z. Wang, T. Kiyokawa, I. Sera, N. Yamanobe, W. Wan, and K. Harada, “Error correction in robotic assembly planning from graphical instruction manuals,” *IEEE Access*, vol. 11, pp. 107 276–107 286, 2023.
- [10] J. Lv, R. Zhang, X. Li, S. Liu, T. Liu, Q. Zhang, and J. Bao, “A multimodality scene graph generation approach for robust human–robot collaborative assembly visual relationship representation,” *IEEE Transactions on Industrial Informatics*, vol. 20, no. 3, pp. 3242–3251, 2024.
- [11] J. Zhao, B. Vogel-Heuser, J. Ao, Y. Wu, L. Zhang, F. Hartl, D. Hujo, Z. Bing, F. Wu, A. Knoll, S. Haddadin, B. Vojanec, T. Markert, and A. Kraft, “Ontology based ai planning and scheduling for robotic assembly,” in *2024 IEEE/RSJ International Conference on Intelligent Robots and Systems (IROS)*, 2024, pp. 9855–9862.
- [12] A. Angleraud, M. Netzev, and R. Pieters, “Knowledge-based planning for human-robot collaborative tasks,” *IEEE Access*, vol. 13, pp. 110 752–110 764, 2025.
- [13] R. K.-J. Lee, H. Zheng, and Y. Lu, “Human-robot shared assembly taxonomy: A step toward seamless human-robot knowledge transfer,” *Robotics and Computer-Integrated Manufacturing*, vol. 86, p. 102686, 2024. [Online]. Available: <https://www.sciencedirect.com/science/article/pii/S0736584523001618>

[14] C. J. Conti, A. S. Varde, and W. Wang, "Human-robot collaboration with commonsense reasoning in smart manufacturing contexts," *IEEE Transactions on Automation Science and Engineering*, vol. 19, no. 3, pp. 1784–1797, 2022.

[15] F. Sun, S. Miao, D. Zhong, L. Wu, H. Zhou, N. Wang, Z. Wen, and H. Huang, "Manipulation skill representation and knowledge reasoning for 3c assembly," *IEEE/ASME Transactions on Mechatronics*, pp. 1–11, 2025.

[16] S. Ji, S. Lee, S. Yoo, I. Suh, I. Kwon, F. C. Park, S. Lee, and H. Kim, "Learning-based automation of robotic assembly for smart manufacturing," *Proceedings of the IEEE*, vol. 109, no. 4, pp. 423–440, 2021.

[17] A. Bashir, R. Moktafi, M. Giangreco, and R. Mueller, "State space exploration with large language models for human-robot cooperation in mechanical assembly," in *2024 7th Iberian Robotics Conference (ROBOT)*, 2024, pp. 1–6.

[18] A. Macaluso, N. Cote, and S. Chitta, "Toward automated programming for robotic assembly using chatgpt," in *2024 IEEE International Conference on Robotics and Automation (ICRA)*, 2024, pp. 17 687–17 693.

[19] J. Ao, F. Wu, Y. Wu, A. Swiki, and S. Haddadin, "Llm-as-bt-planner: Leveraging llms for behavior tree generation in robot task planning," in *2025 IEEE International Conference on Robotics and Automation (ICRA)*, 2025, pp. 1233–1239.

[20] K. Rana, J. Haviland, S. Garg, J. Abou-Chakra, I. Reid, and N. Suenderhauf, "Sayplan: Grounding large language models using 3d scene graphs for scalable task planning," in *7th Annual Conference on Robot Learning*, 2023. [Online]. Available: <https://openreview.net/forum?id=wMpOMO0Ss7a>

[21] H. You, Y. Ye, T. Zhou, Q. Zhu, and J. Du, "Robot-enabled construction assembly with automated sequence planning based on chatgpt: Robogpt," *Buildings*, vol. 13, no. 7, 2023. [Online]. Available: <https://www.mdpi.com/2075-5309/13/7/1772>

[22] M. Forlini, M. Babcinschi, G. Palmieri, and P. Neto, "D-rmrgpt: Robot-assisted collaborative tasks driven by large multimodal models," 2024. [Online]. Available: <https://arxiv.org/abs/2408.11761>

[23] J. H. Kang, N. Dhanaraj, S. Wadaskar, and S. K. Gupta, "Using large language models to generate and apply contingency handling procedures in collaborative assembly applications," in *2024 IEEE International Conference on Robotics and Automation (ICRA)*, 2024, pp. 15 585–15 592.

[24] P. Hao, S. Cui, J. Wei, T. Lu, Y. Cai, and S. Wang, "Learn-gen-plan: Bridging the gap between vision language models and real-world long-horizon dexterous manipulations," *IEEE Transactions on Automation Science and Engineering*, vol. 22, pp. 15 638–15 649, 2025.

[25] M. Deng, B. Fu, L. Li, and X. Wang, "Integrating llms and digital twins for adaptive multi-robot task allocation in construction," 2025. [Online]. Available: <https://arxiv.org/abs/2506.18178>

[26] K. Ramachandruni, C. Kent, and S. Chernova, "Uhpt: A user-aware hierarchical task planning framework for communication-free, mutually-adaptive human-robot collaboration," *J. Hum.-Robot Interact.*, vol. 13, no. 3, Aug. 2024. [Online]. Available: <https://doi.org/10.1145/3623387>

[27] G. Pegoraro, G. Giacomuzzo, M. Terreran, S. Ghidoni, R. Carli, and D. Romeres, "E-uhpt: An enhanced user-aware hierarchical task planning framework for robust human-robot collaboration," in *Proceedings of the IFAC Joint Conference on Computers, Cognition, and Communication*. IFAC, 2025, mERL Technical Report TR2025-134. [Online]. Available: <https://www.merl.com/publications/TR2025-134>

[28] M. Cramer, K. Kellens, and E. Demeester, "Probabilistic decision model for adaptive task planning in human-robot collaborative assembly based on designer and operator intents," *IEEE Robotics and Automation Letters*, vol. 6, no. 4, pp. 7325–7332, 2021.

[29] H. Nemilekar, N. Dhanaraj, A. Guan, S. K. Gupta, and S. Nikolaidis, "Transfer learning of human preferences for proactive robot assistance in assembly tasks," in *Proceedings of the 2023 ACM/IEEE International Conference on Human-Robot Interaction*, ser. HRI '23. New York, NY, USA: Association for Computing Machinery, 2023, p. 575–583. [Online]. Available: <https://doi.org/10.1145/3568162.3576965>

[30] Z. Wang, T. Kiyokawa, N. Yamanobe, W. Wan, and K. Harada, "Assembly task allocation for human–robot collaboration considering stability and assembly complexity," *IEEE Access*, vol. 12, pp. 159 821–159 832, 2024.

[31] Q. Chen and Y.-J. Pan, "An optimal task planning and agent-aware allocation algorithm in collaborative tasks combining with pdl and popf," 2024. [Online]. Available: <https://arxiv.org/abs/2407.08534>

[32] G. Giacomuzzo, M. Terreran, S. Jain, and D. Romeres, "Decaf: a discrete-event based collaborative human-robot framework for furniture assembly," 2024. [Online]. Available: <https://arxiv.org/abs/2408.16125>

[33] I. El Makrini, M. Omidi, F. Fusaro, E. Lamon, A. Ajoudani, and B. Vanderborght, "A hierarchical finite-state machine-based task allocation framework for human-robot collaborative assembly tasks," in *2022 IEEE/RSJ International Conference on Intelligent Robots and Systems (IROS)*, 2022, pp. 10 238–10 244.

[34] Z. Zhou, S. Wang, Z. Chen, M. Cai, H. Wang, Z. Li, and Z. Kan, "Local observation based reactive temporal logic planning of human-robot systems," *IEEE Transactions on Automation Science and Engineering*, vol. 22, pp. 643–655, 2025.

[35] A. Pupa, S. Comari, M. Arrfou, G. Andreoni, A. Carapia, M. Carricato, and C. Secchi, "Enhancing performance in human–robot collaboration: A modular architecture for task scheduling and safe trajectory planning," *IEEE Transactions on Automation Science and Engineering*, vol. 22, pp. 17 535–17 551, 2025.

[36] J. Serra and J. Serra, *Image Analysis and Mathematical Morphology*, ser. Image Analysis and Mathematical Morphology. Academic Press, 1982. [Online]. Available: <https://books.google.com/books?id=BpdTAAAYAAJ>

[37] N. Kiryati, A. M. Bruckstein, and R. Richardson, "A probabilistic hough transform," in *Proceedings of IEEE Conference on Computer Vision and Pattern Recognition (CVPR)*. IEEE, 1991, pp. 155–160.

[38] J. White, Q. Fu, S. Hays, M. Sandborn, C. Olea, H. Gilbert, A. El-nashar, J. Spencer-Smith, and D. C. Schmidt, "A prompt pattern catalog to enhance prompt engineering with chatgpt," *arXiv preprint arXiv:2302.11382*, 2023.

[39] J. Wei, X. Wang, D. Schuurmans, M. Bosma, B. Ichter, F. Xia, E. H. Chi, Q. V. Le, and D. Zhou, "Chain-of-thought prompting elicits reasoning in large language models," in *Proceedings of the 36th International Conference on Neural Information Processing Systems*, ser. NIPS '22. Red Hook, NY, USA: Curran Associates Inc., 2022.

[40] J. B. MacQueen, "Some methods for classification and analysis of multivariate observations," in *Proceedings of the Fifth Berkeley Symposium on Mathematical Statistics and Probability*, vol. 1. University of California Press, 1967, pp. 281–297.

[41] J. Cannby, "A computational approach to edge detection," *IEEE Transactions on Pattern Analysis and Machine Intelligence*, vol. 8, no. 6, pp. 679–698, 1986.

[42] H. Freeman and R. Shapira, "Determining the minimum-area encasing rectangle for an arbitrary closed curve," in *Graphics Gems II*, J. Arvo, Ed. Academic Press, 1991, pp. 34–37.

[43] V. Villani, F. Pini, F. Leali, and C. Secchi, "Survey on human–robot collaboration in industrial settings: Safety, intuitive interfaces and applications," *Mechatronics*, vol. 55, pp. 248–266, 2018. [Online]. Available: <https://www.sciencedirect.com/science/article/pii/S0957415818300321>

[44] M. R. Kolani, S. Nousias, and A. Borrmann, "Coordinating robotized construction using advanced robotic simulation: The case of collaborative brick wall assembly," 2024. [Online]. Available: <https://arxiv.org/abs/2405.17171>

APPENDIX

A. A. Prompt of Match Agent

```

1 ROLE AND TASK OBJECTIVE
2 You are a construction-aware visual reasoning
   specialist for timber-frame structures. Analyze
   the design image, perception rectangles, and
   metadata JSON to determine which components are
   installed. Use step-by-step internal reasoning
   that is hidden but not skipped. Integrate
   geometry, topology, and semantics. Each decision
   must specify the component_id, the matched
   perception ID if any, and a concise justification.
3
4 1. INPUT SPECIFICATIONS
5 1.1 Overview
6 The inputs include: (a) a design image with labeled
   components, (b) a perception image containing
   detected rectangles aligned to the design view,
   and (c) a JSON metadata file defining the types,
   geometry, and topology of each component.
7
8 1.2 Design Image
9 File: "Gable Wall Framing - Frame 1_27
   components.png".
10 Numeric labels indicate single-layer components, and
   fractional labels indicate layered components.
   The labels map directly to JSON dxf_entity_id

```

```

values, for example rect_000 corresponds to label
0 and rect_001 to label 1.

11 12 Design colors are semantically fixed:
13 - Stud is Cyan (0,255,255).
14 - Bottom Plate is Orange (255,165,0).
15 - Top Plate is Yellow (255,255,0).
16 - Header is Red (255,0,0).
17 - King Stud is Blue (0,0,255).
18 - Trimmer is Lime (0,255,0).
19 - Diagonal Brace is Magenta (255,0,255).
20 - Cripple is Violet (138,43,226).
21 - Sill Plate is Green (0,128,0).
22
23 In addition to the color-coded rectangles and numeric
    dxf_entity_id labels, the design image includes
    red text annotations identifying the main
    vertical load-bearing components. These labels
    serve as explicit semantic cues:
24 -Stud labels appear above their numeric ids.
25 -King stud and trimmer labels appear below their
    numeric ids.
26
27 These annotations directly indicate the functional
    category of each vertical member and provide
    additional visual anchors for component
    identification during matching.
28
29 1.3 Perception Image
30 File: "Perception_[ID]_[N] rectangles.png".
31 Rectangles are labeled P0 through P(N-1), obtained
    from RGB-D segmentation. Perception colors follow
    a cycle by index modulo 10 and have no semantic
    meaning.
32
33 1.4 Metadata JSON
34 File: "Gable Wall Framing - Frame 1_Components.json".
35 The root includes frame_id, wall_name,
    construction_constants, and an array of
    components. Each component has:
36 - component_id.
37 - type, chosen from {Top Plate, Bottom Plate, Stud,
    King Stud, Trimmer, Header, Sill Plate, Cripple,
    Diagonal Brace}.
38 - geometry including bounding_box and dimensions in
    inches.
39 - dxf_entity_id.
40 - topology.connected_to.
41 Bounding boxes are in design-image coordinates, and
    dimensions are expressed in inches.
42
43 2. ONTOLOGY AND NAMING
44 2.1 Component Roles
45
46 Bottom Plate is the lowest horizontal member and
    connects all vertical members.
47 Top Plate is the highest horizontal member and
    connects to vertical and brace members.
48 Header is a thick horizontal member above an opening
    and may be flanked by king studs.
49 Sill Plate is a horizontal member below a window.
50 Stud is a vertical member that connects bottom plate
    to top plate, positioned away from openings.
51 King Stud flanks an opening and connects to headers,
    linking bottom plate to top plate.
52 Trimmer is placed inside king studs and supports
    headers or sill plates.
53 Cripple is a short vertical member above headers or
    below sill plates.
54 Diagonal Brace is angled and connects plates and
    studs.
55
56 2.2 Component ID Naming Semantics
57
58 Numeric suffixes (_1, _2, ...) indicate left-to-right
    order within the frame where stud_1 is leftmost
    and stud_N is rightmost.
59 Multi-layer vertical suffixes (_2, _3) indicate inner
    layers positioned closer to the opening interior
    for opening-related vertical components, such as
    trimmer_left_down_2 being the innermost trimmer
    layer.
60 Opening-based positioning terms are relative to
    header position for opening-related components,
    with directional terms left/right and up/down
    based on header or sill plate location.

61 62 3. REASONING METHODOLOGY
63 The reasoning process follows a structured analysis
    framework. The final JSON output derives from
    this reasoning chain.
64
65 3.1 Preprocessing
66 Apply position-based filtering to perception
    rectangles:
67 - Retain rectangles whose relative position in the
        frame suggests structural validity, even if
        partial geometry is detected.
68 - Remove rectangles that appear entirely detached
        from surrounding frame structures, unless their
        location corresponds to a known high-position
        component such as a header.
69 - Apply geometric plausibility filtering: remove
        rectangles with implausible aspect ratios or
        sizes that cannot reasonably represent timber
        components.
70 - Record filtered rectangles for output reporting.
71
72 3.2 Ordered Matching
73 3.2.1 Horizontals (bottom to top)
74 - Identify in order: bottom plate, sill plate,
    header, top plate.
75
76 3.2.2 Verticals (conditional on opening)
77 When header or sill detected:
78 - Define opening bounds from the detected header/sill
    span.
79 - King studs must be adjacent to detected
    headers/sills AND verify topology.connected_to
    relationships.
80 - Inside opening: match verified king studs (flanks),
    then trimmers (inside, up/down), then cripes
    (above header or below sill).
81 - Outside opening: match remaining studs from left to
    right.
82 When no clear opening detected:
83 - Match studs from left to right first.
84 - Then attempt opening-related verticals using design
    metadata bounding_box as reference.
85
86 3.2.3 Diagonals
87 - Search near corners.
88 - Diagonal brace must connect plates and adjacent
    verticals.
89
90 3.3 Conflicts and Constraints
91 When conflicts arise, apply the following rules:
92
93 - Each perception rectangle can only be assigned to
    one component type. Multi-layer components of the
    same type (e.g., header_layer_1, header_layer_2)
    may share one rectangle, but different component
    types cannot share.
94 - Permit segment merging only for aligned segments
    within tolerance and never across different types.
95 - Validate each proposed component match using its
    topology.connected_to relationships.
96 - Ensure all matches respect topology connections and
    ordering, for example stud_1 must be left of
    stud_2.
97
98 3.4 Dependency-Based Installation Inference
99 After completing the ordered visual matching,
    determine the installation status of components
    that may not have been directly detected due to
    environmental factors affecting on-site
    perception:
100 Multi-Layer Installation Rules:
101 When any layer of a multi-layer component (Bottom
    Plate, Top Plate, Header, Sill Plate) is
    detected, all layers of that component are
    considered installed
102 Structural Dependency Rules:
103 - When a header is detected, also infer the presence
        of the opening king studs and the trimmers below
        it.
104 - Such inference is applied only when the opening
        geometry is anchored and no contradictory
        evidence exists.
105 For all inference results, set: match_status

```

```

106     "inferred_installed", matched_to null,
107     inference_type ("multi_layer_inference" |
108     "dependency_inference").
109
109 3.5 Self-Verification
110 Before output, confirm that every component_id has
111     exactly one match_status, all matched_to IDs are
112     valid, and vertical assignments are unique.
113 - Only multi-layer horizontals may share.
114 - Topology must remain consistent.
115 - Verify matched perception rectangles align with
116     corresponding design image components in position
117     and geometry, where the rect_XXX identifier
118     corresponds to the labeled rectangle number in
119     the design image (e.g., rect_022 corresponds to
120     design rectangle labeled "22").
121 - Verify no perception rectangle is assigned to
122     multiple different component types. Check that
123     each matched_to ID appears only once across all
124     different component types.
125 - The JSON must be valid, with no markdown or code
126     fences.
127
128 4. OUTPUT REQUIREMENTS
129
130 The output must be a JSON object with two sections:
131 - filtered_rectangles, which is a list of excluded
132     perception IDs.
133 - component_matches, which is an array of objects.
134     Each object includes component_id, match_status
135     (one of "matched_with_high_confidence",
136     "partial_match", "uncertain_merge",
137     "not_matched", "unclear", "inferred_installed"),
138     matched_to (a perception rectangle ID or null),
139     design_rectangle_id, inference_type (null,
140     "dependency_inference", or
141     "multi_layer_inference"), and a reason.
142
143 Example:
144 {
145     "filtered_rectangles": ["P4"],
146     "component_matches": [
147         {"component_id": "stud_4", "match_status": "matched_with_high_confidence",
148          "matched_to": "P3", "design_rectangle_id": "rect_022", "inference_type": null,
149          "reason": "Vertical span consistent; connects bottom
150                  plate"}
151     ]
152 }
153

```

```

14
15 Step 2. Geometric plausibility
16 - Central-band requirement: For vertical members
16     (studs, trimmers, cripple studs, blocking), only
16     retain rectangles within the central vertical
16     band of the image.
17 - Top plate and bottom plate are exempt from this
17     requirement and may be retained even if spanning
17     the full width.
18 - Abnormal clusters: Rectangles that appear densely
18     packed, overlapped, or glued together without
18     clear spacing are invalid. When such clustering
18     occurs, the entire group must be discarded.
19 - Isolation: Rectangles disconnected from the main
19     frame structure (small fragments, tilted, or
19     misdetections) must be discarded.
20
21 Step 3. Structural exceptions
22 - Short vertical members positioned between two valid
22     horizontals (above a header or below a sill,
22     within the central band) must be retained, even
22     if they appear clustered or partially unclear in
22     the Scene Photo.
23 - These exceptions apply only to centrally located
23     trimmers and cripple studs, not to side stacks or
23     edge clusters.
24
25 3. OUTPUT REQUIREMENTS
26 Only list the IDs of retained rectangles. Do not
26     include explanations or reasons.
27 The output must be a JSON object with one section:
28 - filtered_rectangles, which is a list of retained
28     perception IDs.
29
30 Example:
31 {
32     "filtered_rectangles": ["P0", "P5"]
33 }

```

B. B. Prompt of Filter Agent

```

1 ROLE AND TASK OBJECTIVE
2 You are a construction-aware reasoning assistant.
2     Analyze the perception image together with the
2     corresponding scene photo. Your task is to filter
2     out all invalid perception rectangles and retain
2     only those that plausibly represent installed
2     timber-frame components. The reasoning must
2     follow a clear multi-step filtering process,
2     strictly based on scene-consistent reasoning.
3
4 1. INPUT SPECIFICATIONS
5 Perception Image: an image containing labeled
5     rectangles (P0, P1, ...) detected from RGB-D
5     segmentation.
6 Scene Photo: a real photo taken at the same time
6     showing the actual lumber placement.
7 The two images correspond by ID (e.g.,
7     Perception_T021 corresponds to 021_Color).
8
9 2. FILTERING PROCESS
10 Step 1. Scene-based validation
11 - Keep rectangles only if they correspond to lumber
11     clearly visible in the Scene Photo as part of the
11     emerging frame.
12 - Reject rectangles from stacked, leaning, or
12     misplaced lumber.
13 - Rectangles located at the far left or far right
13     edge zones that form part of a tight stack must
13     be discarded as a whole group (no single
13     rectangle is retained from such a cluster).

```